Journal of Physics: Conference Series **2374** (2022) 012011 doi:10.1088/1742-6596/2374/1/012011

Fast Beam Condition Monitor of the CMS experiment at HL-LHC

Mohammad Sedghi
On behalf of the CMS Collaboration

Department of Electrical and Computer Engineering, Isfahan University of Technology, Isfahan 84156-83111, Iran

E-mail: msedghi@cern.ch

Abstract. To achieve the challenging target of 1% precision for luminosity measurement at the high-luminosity LHC (HL-LHC) with instantaneous luminosity up to $7.5\times10^{34}\,\mathrm{cm}^{-2}\,\mathrm{s}^{-1}$, the CMS experiment will employ multiple luminometers with orthogonal systematics. A key component of the proposed system is a standalone luminometer, the Fast Beam Condition Monitor (FBCM), which is fully independent of the central trigger and data acquisition and hence is able to operate outside of CMS data taking periods at 40 MHz providing bunch-by-bunch luminosity measurement with 1 s time granularity. FBCM will be placed inside the cold volume of the tracker as it utilizes silicon-pad sensors with an asynchronous read-out. A zero-hit-counting algorithm will be used to measure luminosity. FBCM will also provide precise timing information with a few ns precision enabling the measurement of beam-induced background. We report on the optimization of the design and the expected performance of FBCM.

1. Introduction

The motivation for high precision luminosity measurement is driven by the expected precision of physics measurements. For example the total uncertainty of the differential Z-boson production cross section measurement is expected to be less than 1% excluding the luminosity uncertainty [1]. Therefore, luminosity measurements for Phase-2 are targeted to reach a precision of 1% at the high-luminosity LHC (HL-LHC) [2, 3]. To reach this goal, the full potential of CMS instrumentation will be exploited and a dedicated stand-alone luminometer—the Fast Beam Conditions Monitor (FBCM), is also being developed. The FBCM will allow to precisely measure the bunch-by-bunch luminosity of the LHC beams. Being independent of central trigger and data acquisition systems, it can be operated always when there is beam in the machine. Its design is inspired by the successful BCM1F project [4, 5] which has been already developed for data-taking in Run 3 based on AC-coupled double silicon-pad sensors. The current location of the BCM1F subsystem will be occupied by the Tracker Endcap Pixel Detector during Phase-2 of the CMS upgrade. Therefore, the FBCM should be designed for a higher z inside the tracker volume. Readout electronics and detector design of the FBCM will be optimized to reach the challenging luminosity measurement requirements.

The FBCM detector utilizes 336 silicon-pad sensors with a fast asynchronous digital readout and active cooling inside the tracker volume for which the cooling and power supply services are available similar to the inner tracker subsystems [6]. In addition, the FBCM will be able to

measure the beam-induced background (BIB) based on the time separation between the beam-induced particles and the head-on collision products only in bunch-crossing (BX) positions where there is no significant out-of-time afterglow.

2. FBCM architecture and readout protocol

The FBCM is divided into four quarters, where each quarter comprises of half of one end of the detector. The key building blocks of the FBCM are four front-end modules and four hybrid port cards. Figure 1 shows the logical connections among different parts of each FBCM quarter.

Every seven pads are grouped on a silicon die and will be fabricated with the general technologies being developed for the CMS Phase-2 upgrade with AC-coupled connections. The thickness of sensors is assumed similar to that of the inner tracker [6] in order to ensure the sensors' longevity. Each front-end module includes 21 silicon-pad sensors and the relevant electronics. The hybrid port cards [6] receive the front-end output signals and transmit the data to the back-end over optical links. Each hybrid port card includes three lpGBT chips—a chip for low power gigabit transmission [7] in the Phase-2 of CMS—and three versatile link transceivers (VTRx+) [8] to send and receive data via optical fibers. Once a hit is received on a silicon-pad sensor, the generated ionization charge produces a short pulse. The signal will be amplified and shaped in the front-end ASIC, then a non-clocked digital output pulse will be produced, where the rising edge corresponds to the threshold crossing of the amplified analog signal and the duration is equivalent to the time-over-threshold. Within the port cards, the lpGBT continuously samples the output signal of the front-end channels. Then the data will be sent to the back-end by the VTRx module. At the back-end, blades based on Advanced Telecommunications Computing Architecture (ATCA) will be employed to histogram the number of hits per BX. Since the FBCM is based on detecting individual particle hits, it is not able to distinguish between one or more particles hitting the system at the same time. Hence, the hit-counting method is not effective in FBCM. Therefore, the fraction of events with zero-hits per BX is used to estimate the hit rate and the luminosity, assuming that the number of interactions follows the Poisson statistics; such method is known as the zero-counting [9] approach.

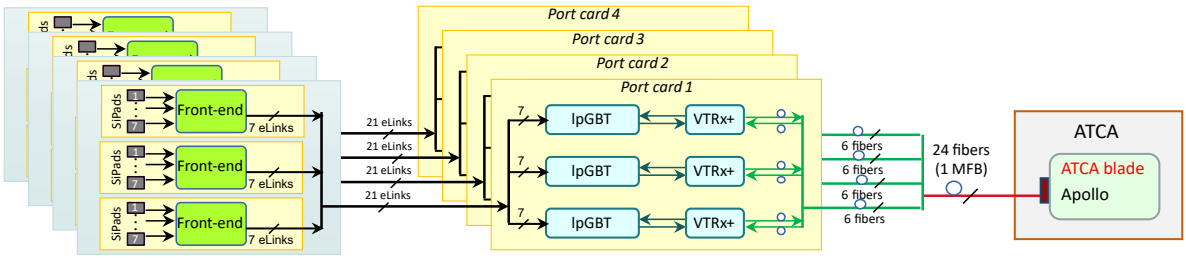

Figure 1. Architecture of a quarter of FBCM. Each FBCM quarter contains 84 silicon sensors and four port cards.

The FBCM is foreseen to be located behind the last disk of the Tracker Endcap Pixel Detector corresponding to $8 < r < 30\,\text{cm}$ and $277 < |z| < 290\,\text{cm}$. The radiation dose at the foreseen location has been estimated using FLUKA [10] and CMSSW (the CMS software framework) [11] resulting in $\approx$3.1 hits/cm^2/BX for a single bunch instantaneous luminosity of $28\,\text{Hz}/\mu\text{b}$ at a radius of $r \approx 14.5\,\text{cm}$. This is acceptable for the zero-counting algorithm implementation. Regarding the hardness of components against the radiation, FLUKA simulations show that the total ionization dose (TID) and the 1 MeV neutron equivalent fluence are less than 175 MRad and $3.2 \times 10^{15}\,\text{cm}^{-2}$, respectively: those are acceptable for the front-end modules and the hybrid port cards.

3. Optimization and expected performance

The size of sensors plays an important role in the performance of FBCM, in terms of both the linearity and the statistical uncertainty. In an ideal scenario where there is no restriction on the electronic components, an analytical study predicts that the statistical uncertainty in the rate could be minimized for the relatively large size of the sensors as shown in Fig. 2. However, such large sensor area is not applicable because probable multiple hits could be missed due to the limited temporal response of the front-end electronics, resulting in nonlinearity. According to Fig. 2 which is based on an analytical analysis at the foreseen location of the FBCM detector for the average pileup of 200, one can find that the rate uncertainty, at an ideal and ultimate case, cannot be lower than 0.064%. Nevertheless, such level of uncertainty is not achievable in practice, and a decent accurate simulation is required in order to include the limitations of electronics for sensor size optimization.

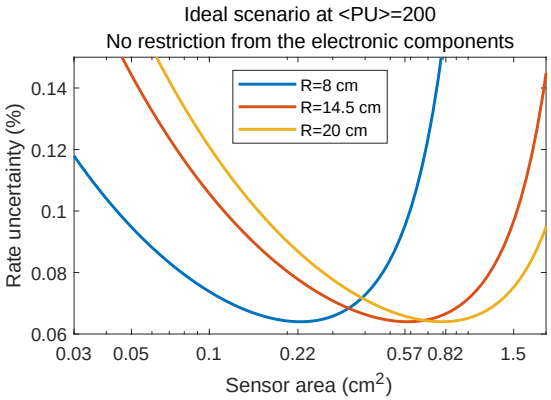

Figure 2. The rate uncertainty at average pileup of 200 as a function of variation of each sensor size, assuming 336 sensors located at the foreseen location of the FBCM. The horizontal axis is in logarithmic scale. This plot is based on an analytical study with an ideal scenario that excludes the electronics limitations. The sensor area minimizing the rate uncertainty is not practical, since such values lead to nonlinearity.

In order to find a more accurate estimation for the appropriate size of the sensors as well as the placement radius, full CMSSW simulations based on the GEANT4 [12] framework and using a behavioral model for the front-end electronics with a customized digitizer (tuned with the BCM1F front-end [13] and equipped with a constant fraction discriminator), were carried out. Eight different sensor sizes (i.e., 2.25, 2.89, 3.85, 5.37, 8.02, 13.27, 26 and 72.22 mm^2) and positions at different r, spanning the range from 8 to 20 cm, were investigated to find out the optimal detector performance.

Figure 3 shows the deviation from linearity and the statistical uncertainty as function of various choices of sensor sizes and placement radius with average pileup of 200, corresponding to the worse case scenario of leveled instantaneous luminosity of $7.5\times10^{34}\,\mathrm{cm}^{-2}\,\mathrm{s}^{-1}$ at the HL-LHC. The linearity of the mean number of hits per BX per sensor (λ) estimated by the zero-counting approach in FBCM was evaluated in CMSSW as a function of average pileup, $\langle\mathrm{PU}\rangle$. To determine the deviation from linearity, the mean number of hits per sensor per BX as a function of pileup was fitted with a straight line from (0,0) covering the $\langle\mathrm{PU}\rangle$ = 0.5, 1, 1.5, and 10. The slope has a post-fit error of 0.1%. The nonlinearity is calculated as the relative difference between the simulated λ and the values of the fit function at $\langle\mathrm{PU}\rangle = 200$.

As can be seen in Fig. 3, the statistical uncertainty and the linearity are worse for large sensors. On the other hand, for the very small sensor sizes, even a good linearity is achievable, but the rate uncertainty will be increased. Therefore, there will be a trade-off between the rate uncertainty and the linearity. For example, with the sensor size of 2.89 mm^2 as a case study, it is possible to reach λ with deviation less than 0.1% and the rate uncertainty about 0.18% at $\langle\mathrm{PU}\rangle = 200$.

Another potential strength of the FBCM detector is the capability of beam-induced background (BIB) measurement, based on time separation between the incoming particles and

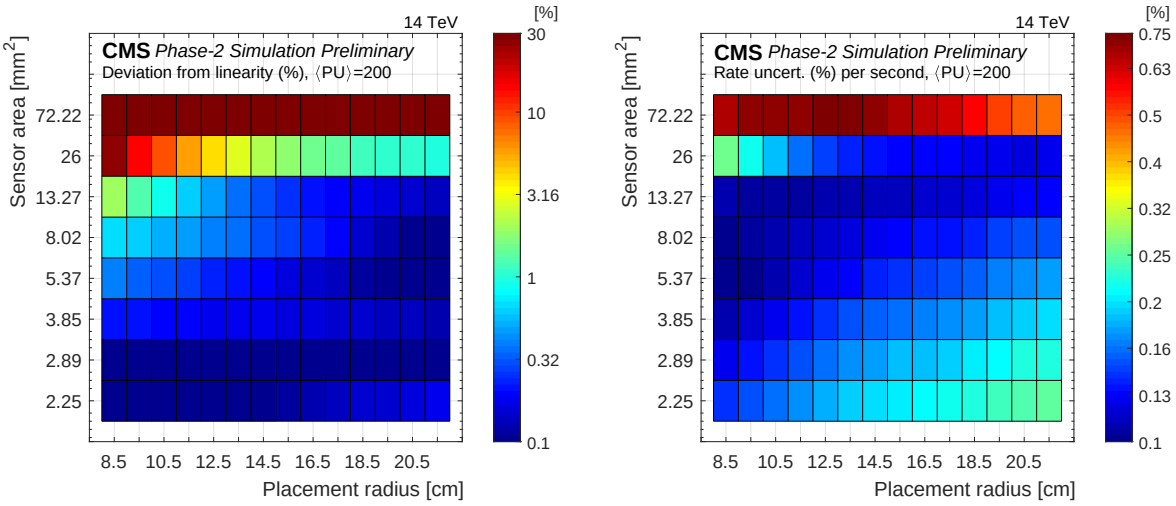

Figure 3. Deviation from linearity (left) and statistical uncertainty of the rate (right) both evaluated at $\langle \mathrm{PU} \rangle = 200$, for different sensor sizes and placement radii, assuming 336 sensors in FBCM. For better illustration, the color bars are presented in logarithmic scale.

BIB reaching the detector either at the beginning of a bunch-train or along with a bunch position where there is a sufficiently long time without collisions that the afterglow contribution is small. Assuming that the beam passes from the left to the right of the detector, the beam-induced particles first reach the $-z$ end of the detector at time-of arrival (ToA) around 6 ns (meaning that 6 ns after the previous BX). Upon traversing through the other end of the detector, the incoming collision products and the BIB could appear at ToA= 0 ns. Given that the timing information of the hits are also sent to the back-end, the FBCM has the capability of recognizing the incoming beam-induced particles from the head-on collision products for the BIB measurement. Such effects have been simulated with CMSSW with input from FLUKA simulations of beam interactions with LHC collimators and various residual beam gas atoms (carbon dioxide, oxygen, and hydrogen). Figure 4 (upper panel) illustrates the timing definitions, time-of-flight (ToF) and ToA, and the lower panel shows the simulated ToF and ToA of beam-induced particles at both ends of FBCM. By using the time binning of around 0.78 ns, it is possible to distinguish the beam-induced particles that reach the FBCM detector only 6 ns after the in-time collision products, and hence BIB could be estimated.

4. Summary

The CMS upgrade coordination endorsed the design of a standalone luminometer for the Phase-2 upgrade of the CMS. The FBCM detector has been proposed and studied as an independent luminometer based on 336 silicon-pad sensors with digital readout, sub-nanosecond resolution, and data transfer rate of 40 MHz. The building blocks of the FBCM and the readout protocol have been introduced. FBCM benefits from the simplicity of the zero-counting algorithm and is also able to transmit the time-of-arrival and time-over-threshold which provides the additional capability to measure beam-induced background. It was shown that the restrictions on the electronic components, e.g., the limited temporal response, lead to nonlinearities, meaning a smaller size of sensors approximates an ideal situation in terms of linearity. As a case study, the expected performance of the FBCM with 336 silicon-pad sensors, 2.89 mm^2 each, corresponds to rate uncertainty of 0.18% and deviation from linearity less than 0.1% at average pileup of 200.

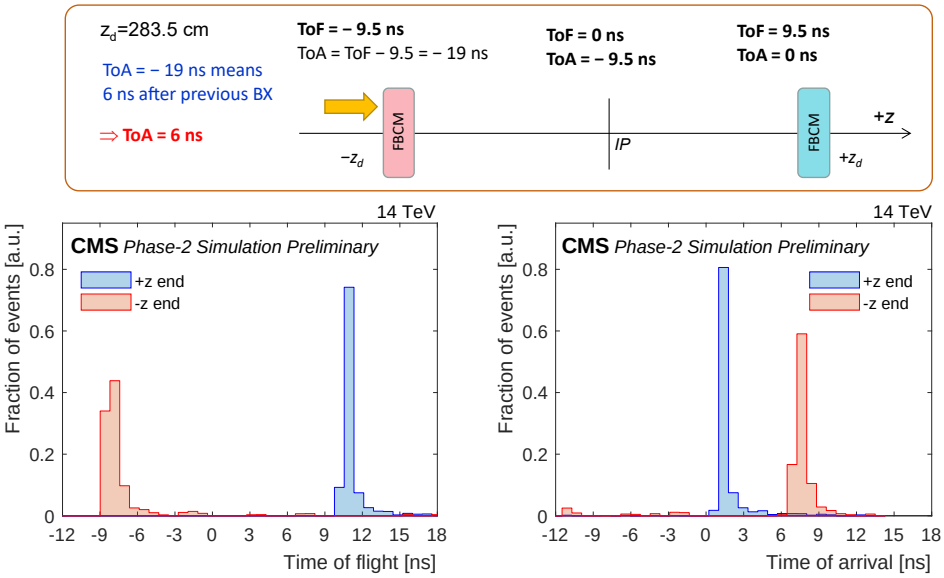

Figure 4. The upper panel illustrates the definition of the time-of-flight (ToF) and time-of-arrival (ToA) variables. ToA represents the delay with respect to a reference time when the products of in-time collisions arrive at the detector. The ToF indicates the time after the nominal collision time at the interaction point. The time-of-flight (lower left) and time-of-arrival (lower right) of beam-induced particles at each end of the FBCM, for sensors with an area of 2.89 mm^2 and located at $r = 14.5$ cm.

Acknowledgments

Thanks to the members of the CMS beam radiation instrumentation and luminosity (BRIL) project and the colleagues at Isfahan University of Technology whose guidance made this possible.

References

[1] CMS Collaboration (CMS) 2021 The Phase-2 Upgrade of the CMS Beam Radiation Instrumentation and Luminosity Detectors Tech. rep. CERN Geneva URL `https://cds.cern.ch/record/2759074`
[2] CMS Collaboration (CMS) 2020 The Phase-2 Upgrade of the CMS Beam Radiation Instrumentation and Luminosity Detectors Conceptual Design CMS Public Note CMS-NOTE-2019-008 CERN URL `https://cds.cern.ch/record/2706512`
[3] CMS Collaboration (CMS) 2015 Technical Proposal for the Phase-II Upgrade of the CMS Detector Tech. rep. CERN Geneva URL `https://cds.cern.ch/record/2020886`
[4] Leonard J L *et al.* 2014 *Nucl. Instrum. Meth. A* **765** 235 (*Preprint* `1405.1926`)
[5] Guthoff M (CMS) 2019 *Nucl. Instrum. Meth. A* **936** 717
[6] CMS Collaboration (CMS) 2017 The Phase-2 Upgrade of the CMS Tracker Technical Design Report CERN-LHCC-2017-009, CMS-TDR-014 CERN URL `https://cds.cern.ch/record/2272264`
[7] Moreira P *et al.* 2019 *Topical Workshop on Electronics for Particle Physics* URL `https://indico.cern.ch/event/799025/contributions/3486153/`
[8] Troska J, Brandon-Bravo A, Detraz S, Kraxner A, Olanterä L, Scarcella C, Sigaud C, Soos C and Vasey F 2017 *PoS* **TWEPP-17** 048. 5 p URL `https://cds.cern.ch/record/2312396`
[9] Odell N J 2012 *36th International Conference on High Energy Physics* (Proceedings of Science)
[10] Ferrari A, Sala P R, Fassò A and Ranft J 2005 FLUKA: A multi-particle transport code (program version 2005) Tech. Rep. CERN-2005-010, SLAC-R-773, INFN-TC-05-11 CERN URL `https://cds.cern.ch/record/898301`
[11] CMS Collaboration (CMS) 2006 CMS Physics: Technical Design Report Volume 1: Detector Performance and Software Tech. rep. CERN Geneva URL `https://cds.cern.ch/record/922757`
[12] Agostinelli S *et al.* (GEANT4) 2003 *Nucl. Instrum. Meth. A* **506** 250
[13] Przyborowski D, Kaplon J and Rymaszewski P 2016 *IEEE Transactions on Nuclear Science* **63** 2300–2308